Electronic Supplementary Information

for Journal of Materials Chemistry B

Metal chelate grafting at the surface of mesoporous silica nanoparticles (MSNs): physico-chemical and biomedical imaging assessment

Myriam Laprise-Pelletier [a,b,d], Meryem Bouchoucha [a,c,d], Jean Lagueux [a], Pascale Chevallier [a,d], Roger Lecomte [e], Yves Gossuin [f], Freddy Kleitz [c,d,*], Marc-André Fortin [a,b,d,*]

[a]Centre de recherche du Centre hospitalier universitaire de Québec (CR-CHUQ), axe Médecine Régénératrice, Québec, G1L 3L5, QC, Canada

[b]Department of Mining, Metallurgy and Materials Engineering, Université Laval, Québec, G1V 0A6, QC, Canada

[c]Department of Chemistry, Université Laval, Québec, G1V 0A6, QC, Canada

[d]Centre de recherche sur les matériaux avancés (CERMA), Université Laval, Québec, G1V 0A6, QC, Canada

[e]Sherbrooke Molecular Imaging Center, CRCHUS, and Department of Nuclear Medicine and Radiobiology, Université de Sherbrooke, Sherbrooke, J1H 5N4, QC, Canada

[f]Service de physique biomédicale
Université de Mons, Mons, B7000, Belgium

*Corresponding authors
E-mail: marc-andre.fortin@gmn.ulaval.ca
E-mail: freddy.kleitz@chm.ulaval.ca

M48SNs and DTPA-M48SNs textural properties. Low-angle powder XRD measurements were carried out on a Siemens D5000 system (Munich, Germany) using Cu Kα radiation (1.541 Å) and operated at 40 kV with a variable slit width. The scanning rate was set over 2θ from 1° to 8°. The Jade (v 2.1) software coupled with JCPDS and ICDD (2001 version) databases was used to analyze the XRD data. The low-angle XRD profile of DTPA-M48SNs showed a broad and weak peak at 2.7° 2θ assigned to the (211) plane of the 3-D cubic $Ia\bar{3}d$ mesostructure (Fig. S1).[1]

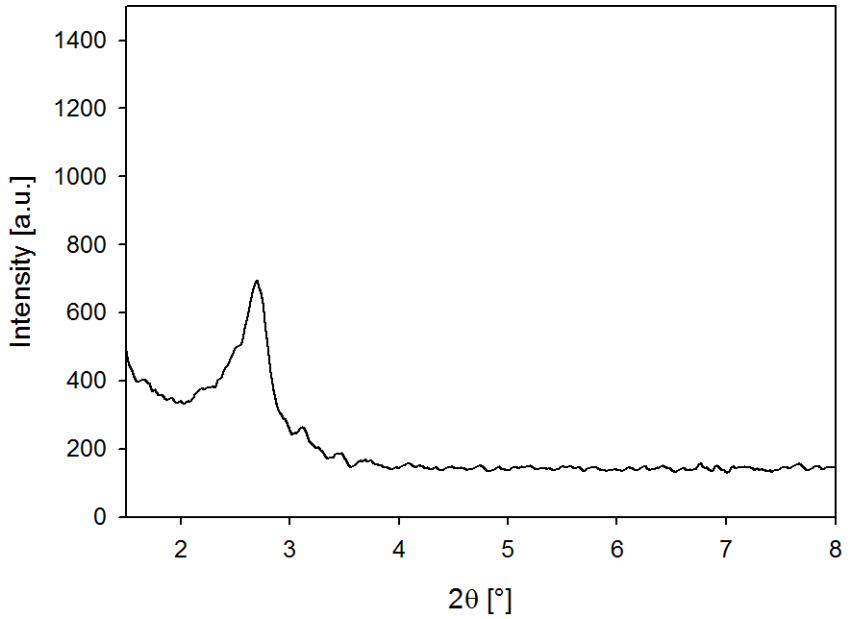

Fig. S1 Low-angle XRD profile of DTPA-M48SNs.

The textural properties and the porosity features were also investigated by N_2 physisorption measurements and porosimetry calculations (Fig. S2-S3 and Table S1). Nitrogen physisorption measurements were performed at −196 °C with an ASAP 2010, Micromeritics (Norcross, GA, USA). Before the sorption measurements, the samples were out-gassed under vacuum for at least 6 hours at >80 °C. The specific surface area (S_{BET}) was determined using the BET equation in the range $0.05 \geq P/P_0 \geq 0.20$ and the total pore volume was obtained at $P/P_0 = 0.95$.

Pure M48SNs showed a type-IV isotherm (IUPAC classification), characteristic of highly ordered M48SN with cylindrical-like pores (Fig. S2). However, the isotherms of DTPA-

M48SNs showed type I-like behavior, which is similar to what is typically found for microporous materials. This behavior can be attributed mainly to the presence of DTPA, not only at the outer surface but also at the entrance of pore channels.

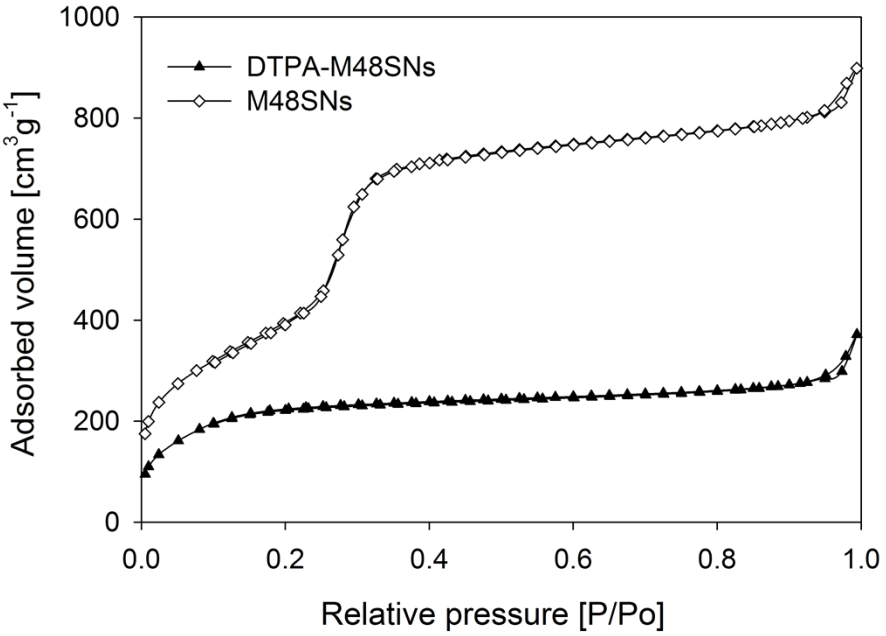

Fig. S2 N_2 physisorption isotherms of DTPA-M48SNs and M48SNs.

The pore size distributions were calculated using non-local density functional theory (NLDFT) methods applying the adsorption branch model (from N_2 physisorption isotherms data and considering N_2 sorption at −196 °C in silica with cylindrical pore geometry). This calculation was performed with Autosorb 1.55 software (Quantachrome Instrument, Boynton Beach, FL, USA). The calculated pore width showed a pronounced decrease after DTPA grafting, from 3.6 to 2.4 nm (Fig. S3).

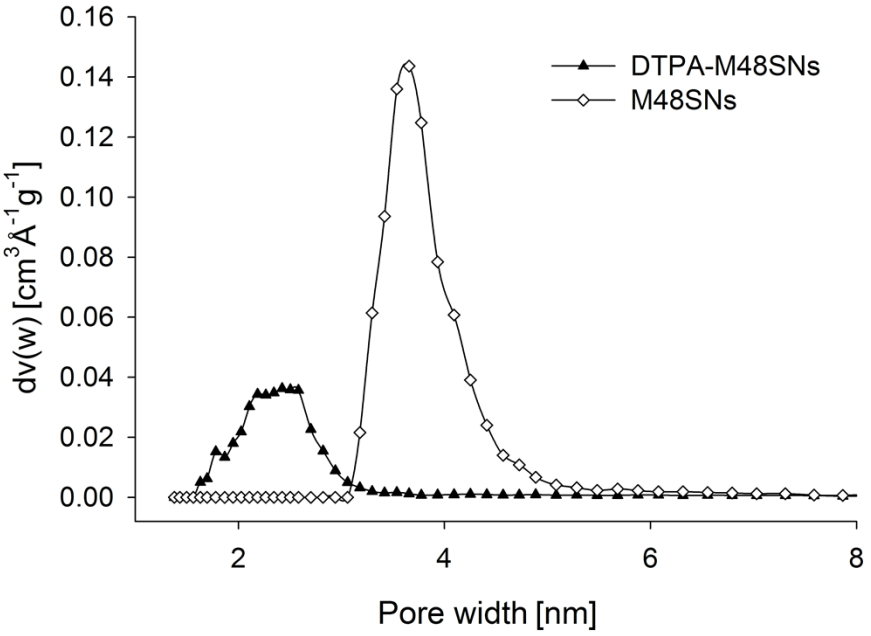

Fig. S3 NLDFT pore size distributions (N_2, 77 K).

DTPA grafting quantification. The amount of attached DTPA molecules was quantitatively determined by thermogravimetric analysis (TGA, Fig. S4). Thermogravimetric analyses were carried out on DTPA-M48SNs using a Netzsch STA 449C thermogravimetric analyzer (Selb, Germany), under air flow of 20 mL/min with a heating rate of 5 °C min^{-1}, between 35 °C and 700 °C. The percentage of grafted molecules (DTPA-APTES) was calculated based on the mass loss between 160 °C and 650 °C. This temperature range excludes solvent (e.g., physisorbed water) and supplementary silica condensation from the calculation (Fig. S4). The unfunctionalized sample, M48SNs, exhibits a loss of 7% w/w attributed to the residual ethoxy groups formed during the surfactant extraction process. After amine and DTPA functionalization, the weight loss was 18.5% and 33.5% (from 160 °C to 650 °C, respectively). Therefore, the amount of organic loss attributed to DTPA, is estimated to about 15% (w/w), confirming thereby the efficiency of DTPA grafting.

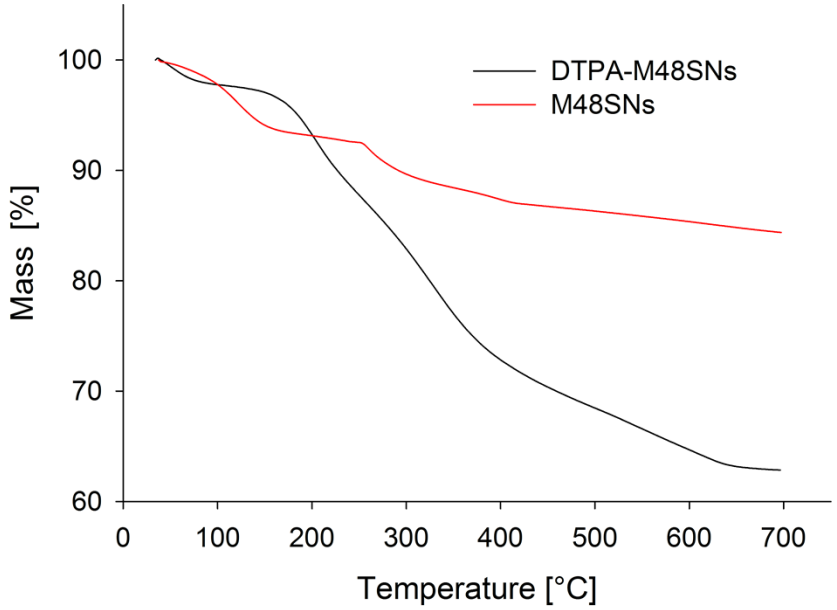

Fig. S4 Thermogravimetric profiles of M48SNs and DTPA-M48SNs.

Relaxometric studies of Gd^{3+}-DTPA-M48SNs. The relaxometric performance of Gd^{3+}-DTPA-M48SNs is shown in Table S1, and compared with the few other Gd-labeled MSNs systems (based on 2D-porosity materials), reported thus far in the literature.

Table S1 Relaxivities of Gd-chelated MSN materials

Sample	Pore network geometry	Temperature [°C]	Magnetic field T, [MHz],	r_1 [$mM^{-1}s^{-1}$]	r_2 [$mM^{-1}s^{-1}$]	r_2/r_1	References
Gd^{3+}-DTPA-M48SNs	3D	37	1.41 [60]	17.6	35.3	2.0	This work
Dye@MSN@Gd@^{64}Cu	2D	-	7 [297.9]	-	-	-	[2]
Gd-MSNs	2D	-	3 [127.7]	19.0	46.8	2.5	[3]
GdL/MCM-41	2D	37	0.47 [20]	27	-	-	[4]
Gd-Dye@MSN	2D	-	0.47 [20]	23	34	1.5	[5]
Gd-DTPA (Magnevist®)	-	37	1.5 [63.8]	3.3	3.9	1.2	[6]

In vitro assessment of contrast media with MRI. Aliquots of diluted Gd^{3+}-DTPA-M48SNs (500 µL) were pipetted in 500 µL-polyethylene centrifugation tubes. The tubes were immersed in water, inserted in a 60-mm RF coil and imaged at 25 °C with a 1 T small-animal MRI system (M2M, Aspect Imaging, Netanya, Israel). T_1-weighted 2D

spin-echo sequences were used, as follows: TE/TR = 14/700 ms; f_α=90°; FOV: 80 mm; 1.4 mm slices with 0.1 mm gap; dwell time 16 μs, matrix: 400 X 400; 3 NEX.

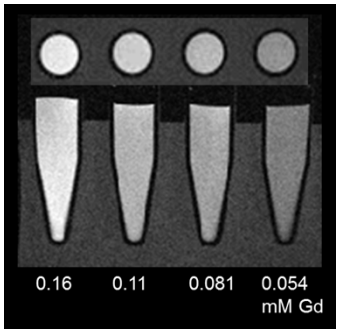

Fig. S5 T_1- weighted MR images of aqueous dilutions of Gd^{3+}-DTPA-M48SNs.

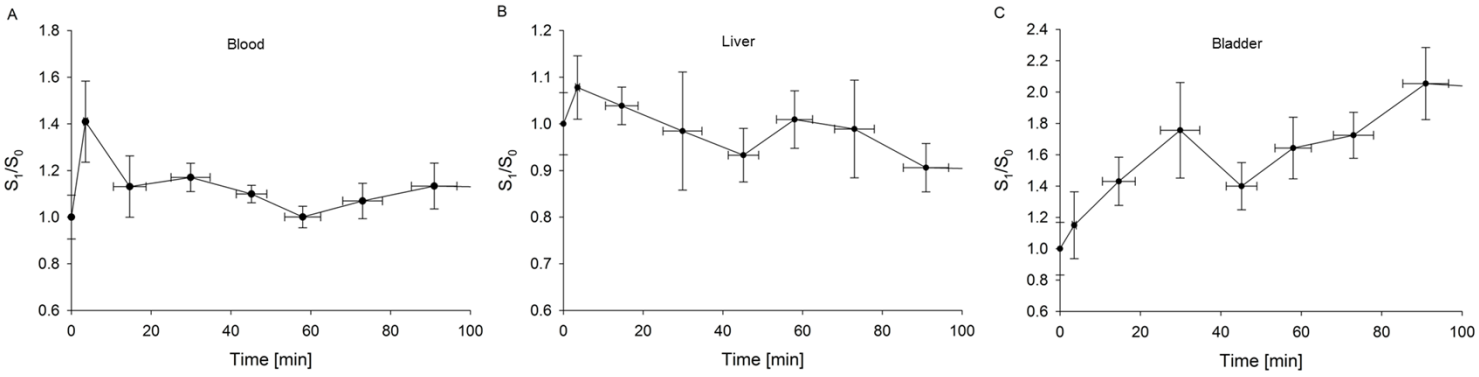

Fig. S6 Dynamic blood clearance profile measured by MRI (**A**), the signal enhancement ratio (S_1/S_0) was calculated for liver and bladder, and plotted in (**B**) and (**C**).

Preparation of $^{64}Cu^{2+}$ radioisotope solution. The radioisotope $^{64}Cu^{2+}$ ($t_{1/2}$ = 12.7 h) was purchased from the Sherbrooke Molecular Imaging Center of CRCHUS (Quebec, Canada), in the form of copper acetate ($^{64}Cu^{2+}(CH_3CO_2)_2$). It was prepared on a TR-19 cyclotron (Advanced Cyclotron Systems, Richmond, BC, Canada) by the reaction $^{64}Ni(p,n)^{64}Cu$ using an enriched ^{64}Ni target electroplated on a solid rhodium disc (22 mm diameter, 1 mm thickness). ^{64}Ni was purchased from Isoflex (San Francisco, CA, USA). $^{64}Cu^{2+}$ was recovered from the target material following the procedure of McCarthy et al.[7] and dispersed in 0.5 mL of 0.1 M HCl. Then, the sample was evaporated and reconstituted in 0.1 M acetate buffer (0.5 mL, pH 5.5). All solutions were prepared with ultrapure water (>18.0 MΩ-cm resistivity).

PET images reconstruction and analysis. Images were reconstructed by MLEM 3D (15 iterations, no attenuation correction) and analyzed with the software LabTEP (Université de Sherbrooke). ROIs were drawn on 3 adjacent transaxial planes, selected on areas covering the liver, the spleen and the kidneys. On each ROI, the average count per second per pixel (Cts/sec/Pix) and the maximum 4 pixel count (MAX4Pix, average of the 4 most intense pixels in ROI) were noted. These values were then corrected for ^{64}Cu decay (12.7 h) referred to the time of injection (t = 0). Then, values in (Cts/sec/Pix) were converted in (Cts/sec/cc) by dividing by the corresponding pixel volume (1.475×10^{-3} cc). The values in (Cts/sec/cc) were then converted in MBq/cc using a calibration factor of (1 Cts/sec/cc = 640.9 Bq/cc), determined by scanning a standard phantom containing a known solution of ^{64}Cu obtained from the cyclotron facility, and measured on the same day. Values in MBq/g were obtained assuming a tissue density of 1g/cc. The percentage of injected dose per g of tissue (%ID/g) was calculated by dividing the values in MBq/g, by the total activity per mouse measured in a well counter (Capintec, Inc., Ramsey, NJ, USA). The dose values were all corrected for decay using the reference time corresponding to the first dynamic scan, for each mouse.

References

1. V. Alfredsson and M. W. Anderson, *Chemistry of Materials*, 1996, **8**, 1141-1146.
2. X. L. Huang, F. Zhang, S. Lee, M. Swierczewska, D. O. Kiesewetter, L. X. Lang, G. F. Zhang, L. Zhu, H. K. Gao, H. S. Choi, G. Niu and X. Y. Chen, *Biomaterials*, 2012, **33**, 4370-4378.
3. J. L. Vivero-Escoto, K. M. L. Taylor-Pashow, R. C. Huxford, J. Della Rocca, C. Okoruwa, H. Y. An, W. L. Lin and W. B. Lin, *Small*, 2011, **7**, 3519-3528.
4. F. Carniato, L. Tei, W. Dastru, L. Marchese and M. Botta, *Chemical Communications*, 2009, 1246-1248.
5. J. K. Hsiao, C. P. Tsai, T. H. Chung, Y. Hung, M. Yao, H. M. Liu, C. Y. Mou, C. S. Yang, Y. C. Chen and D. M. Huang, *Small*, 2008, **4**, 1445-1452.
6. M. Rohrer, H. Bauer, J. Mintorovitch, M. Requardt and H. J. Weinmann, *Investigative Radiology*, 2005, **40**, 715-724.
7. D. W. McCarthy, R. E. Shefer, R. E. Klinkowstein, L. A. Bass, W. H. Margeneau, C. S. Cutler, C. J. Anderson and M. J. Welch, *Nucl Med Biol*, 1997, **24**, 35-43.